Research and Reviews in Materials Science and Chemistry
Vol. 6, Issue 1, 2016, Pages 1-23
ISSN 2319-6920
Published Online on March 30, 2016

http://jyotiacademicpress.net

MODIFICATIONS IN C-S-H COMPOSITION OF CEMENT PASTES WITH SILICA ADDITIONS UNDER DIFFERENT MIXING CONDITIONS

D. ALONSO-DOMÍNGUEZ[1,2], I. ÁLVAREZ-SERRANO[3], E. REYES[2] and A. MORAGUES[2]

[1]CEI Moncloa, UCM-UPM
Edificio del Real Jardín Botánico Alfonso XIII
Madrid, E-28040 Madrid
Spain
e-mail: danielad@quim.ucm.es

[2]Dpto. Ingeniería Civil: Construcción
ETSI de Caminos, Canales y Puertos
Universidad Politécnica de Madrid
E-28040 Madrid
Spain

[3]Dpto. Química Inorgánica I
Facultad Ciencias Químicas
Universidad Complutense de Madrid
E-28040 Madrid
Spain

Keywords and phrases: cement paste, silica fume, SEM, spectroscopy, calcium-silicate-hydrate (C-S-H).

Communicated by Laura Floroian.

Received February 24, 2016; Revised March 16, 2016

Abstract

The modification of the C-S-H gel composition depending on the mixing conditions in two sets of cement paste additivated samples (manual mixed or previously deposited AW and AC) is studied, from ^{29}Si MAS-NMR, ^{27}Al MAS-NMR, FTIR, MIP, EDS, and SEM experiments. In the AW samples no isomorphical Al^{3+} substitution in the silicate chains takes place, whereas for the AC samples $Q^2(1Al)$ signals prompted to the existence of aluminosilicate chains, in which Al^{3+} cations are located in bridging positions of silicate chains. The variations found in the NMR spectra connected to microstructural features and MIP data.

1. Introduction

The use of nanosilica additions in cement-based materials has actually attracted much attention in the last decade. Nanosilica together with several different oxides is among the most employed additions [1-3]. The main searched targets in obtaining new materials depend on the type of nanoparticle chosen. Thus, nanosilica and nanoalumina addition mainly aims to improve the characteristic properties of cement paste materials: enhancement of mechanical compressive strength, densification of the aggregates/paste interface, decrease of the permeability and therefore optimization of durability, etc [4, 5]. Besides this, other additions of metallic oxides concentrate in eventual functional abilities of the material. In this sense, it is worth citing titanium oxide, whose role connected to cement self-cleaning has been widely tested and numerous examples, including specific applications, have been already reported [6]. Iron oxide constitutes another promising additive which concentrates the attention of interesting research concerning the magnetic behaviour and possible applications [7]. In all cases, one of the main difficulties arises for their application due to operational problems associated with the difficulty in workability. In order to optimize the addition efficiency, a good dispersion inside the material is required, and this implies to ensure a good dispersion of particles in the mixing water and a subsequent successful compaction of the material.

In previous works, we have reported on the changes produced in the hydration process of cement pastes with additions of nano and micro silica, obtained under two different addition methodologies [8]. In the first method, the samples prepared by means of the dispersion of particles in the mixing water, in the second method the cement is additivated with the silica (nano and micro size). Several interesting differences in C-S-H gels developing in different cases were observed, and they were related to probable compositional features concerning the mechanism in which aluminum cations are incorporated. In order to tune the most representative properties of the cement-type specimens, especially durability and mechanical compressive strength, it is very important to understand the inner characteristics of the hydration mechanisms, i.e., the principal hydration products stabilized as a function of preparation conditions, taking place in cement paste-derived specimens when hydrated. In recent past years, numerous researches have used the ^{27}Al NMR technique for testing the nature of the different C-S-H gels formed [9-11] and they have proposed structural models of these gels based on the dreierkette structure [12, 13]. With the aim of verifying our previous hypothesis and to get deeper insight about the implied processes, we have now carried out some ^{29}Si MAS NMR, ^{27}Al MAS NMR, MIP, EDS, and SEM experiments and we present in this paper the most relevant results obtained.

2. Material and Methods

2.1. Materials

The plain cement paste (PCP) used as base and reference material is an Ordinary Type I 52.5R Portland cement, which composition is indicated in Table 1. In this study, two sets of samples have been studied. The samples of the first set (denoted AC) were prepared starting from anhydrous cement in which the additions were already incorporated, whereas in the samples of the second set (denoted as AW) the additions

were included during the mixing process. All the phases were prepared at a water-cement ratio w/c = 0.4 using different concentrations of two types of additions: commercial silica nano particles (dry powder), supplied by Cab-O-sil® and micro particles (silica fume), supplied by Ferroatlantica SL. In Table 1, the details of their compositions are also gathered. The selected concentrations were, for both sets of samples, 4 and 10% of nano silica (denoted with N) and 5 and 10% of micro silica (denoted with F). In the notation of water manual mixed samples, i.e., AW ones, a "MA" is included at the end of the name in order to avoid ambiguity.

Table 1. Composition of employed materials

(*Loss on ignition percentage)

Analyte (%)	**Portland Cement CEM I 52.5R**	**Silica Fume**	**Nanosilicacab-o-sil ®**
SiO_2	19.20	95.37	99.9
Al_2O_3	6.07	0.34	0.05
Fe_2O_3	1.70	0.16	0.003
CaO	63.41	0.08	
MgO	2.56	0.04	
SO_3	3.38	0.15	
K_2O	0.82	0.30	
Na_2O	0.33	0.18	
TiO_2			0.03
LOI*	2.09	2.70	1.00

For the AW specimens, the method employed is a variation of that described in the UNEEN 196-1: 2005 norm [14], using 60 hits in a compacting unit. The samples were cast into $1 \times 1 \times 6$cm prisms using steel moulds, where they stayed for 24h in a chamber at 20ºC and 100% humidity. Then they were unmoulded and introduced again into the chamber until the desired curing age: 2, 7, and 28 days. After the

required time, the samples were removed and soaked in is opropanol for 24 hours, and after in a stove at 40ºC for 24 hours, in order to stop the hydration. The characteristics and notation of the studied samples are indicated in Table 2.

Table 2. Mix proportions and notation of specimens. Cem: cement, SF : silica fume, NS : nanosilica, W : water, SP : superplasticizer

Probes	Cem(g)	SF(g)	NS(g)	W(g)	SP(%)
PCP	450	–	–	180	–
4N	432	–	18	180	–
10N	405	–	45	150	4.8
5F	427.5	22.5	–	180	–
10F	405	45	–	180	–
4NMA	432	–	18	180	–
10NMA	405	–	45	150	4.8
5FMA	427.5	22.5	–	180	–
10FMA	405	45	–	180	–

2.2. Methods

Solid state ^{29}Si and ^{27}Al MAS-NMR (Magic Angle Spinning Nuclear Magnetic Resonance) spectroscopy was used to characterize the molecular composition and structure of the hydrated samples. The experiments were carried out on a Bruker Avance 400MHz spectrometer, with a 9.39 T wide bore superconducting magnet, operating at 79.49MHz, with spin rate of 12KHz, 90º; pulse length of 4.5 and 4.0 μs for ^{29}Si and ^{27}Al measurements, respectively.

Scanning electron microscopy (SEM) was performed using a JEOL JSM6335FEG, with resolution of 12Å. Samples were metallized by covering with Au. Semiquantitative chemical analyses were made from energy dispersive X-ray spectroscopy (EDS).

Infrared spectra were recorded on a FTIR Thermo Nicolet 200 spectrophotometer with samples as KBr pellets in the $4000\text{-}400\text{cm}^{-1}$ region.

Mercury intrusion porosimetry (MIP) tests were carried out on Micromeritics Auto pore IV 9500 using an ASTM D 4404-84 [15]. When a curing time of 28 days was reached, solid specimens of about 2-4g were taken from the middle third of the samples. Specimens were oven dried at 40ºC until they reached constant weight. Testing was performed using a mercury porosimeter with a pressure range from subambient to 33.000 psi. The contact angle and surface tension of mercury were assumed to be 130º and 0.485N/m, respectively, for the oven-dried samples.

3. Results and Discussion

As we have previously reported [8], two sets of nano and microsilica additivated cement pastes were prepared by two different mixing methods and were studied at curing ages of 2, 7, and 28 days. Interestingly, it was observed that the AC deposition mixing method improved the samples hydration, mean chain length and polymerization parameters, and this was interpreted in terms of possible different mechanisms implied in each case. In order to investigate this hypothesis, several NMR, MIP, FTIR, and SEM new experiments have been carried out.

3.1. ^{27}Al and ^{29}Si NMR experiments

Previous ^{29}Si NMR experiments seemed to indicate that in the manual mixed samples no isomorphical Al^{3+} substitution in the silicate chains takes place, whereas for the AC samples the obtained signals prompted to the existence of aluminosilicate chains. In order to get deeper insight about these structural details some ^{27}Al NMR experiments have been carried out. This technique permits to determine the different Al species present in cement paste, having in mind that they can be separated when appearing in three typical ppm regions [16-18]:

-Al (IV), tetrahedral coordinated appearing between 50 and 100ppm;

-Al (V), pentahedral coordinated appearing between 30-40ppm range;

-Al (VI), octahedral Al cations, emerging in the 10-20ppm interval.

TGA/DTA data showed [8] the existence of two types of gel, depending on the way the addition is incorporated into the cement paste specimens, as different bands appear in the region corresponding to the C-S-H water loss area.

Figures 1 and 2 comparatively show the corresponding ^{27}Al and ^{29}Si NMR spectra for the samples 10N and 10NMA at a curing age of 28 days, as representative examples of specimens belonging to each set of sample prepared (AC and AW). In them the experimental curves are shown together with the individual and sum calculated ones. The fitting curves have been obtained from smoothed Lorentzian curves, optimized respect to the calculation previously given [8].

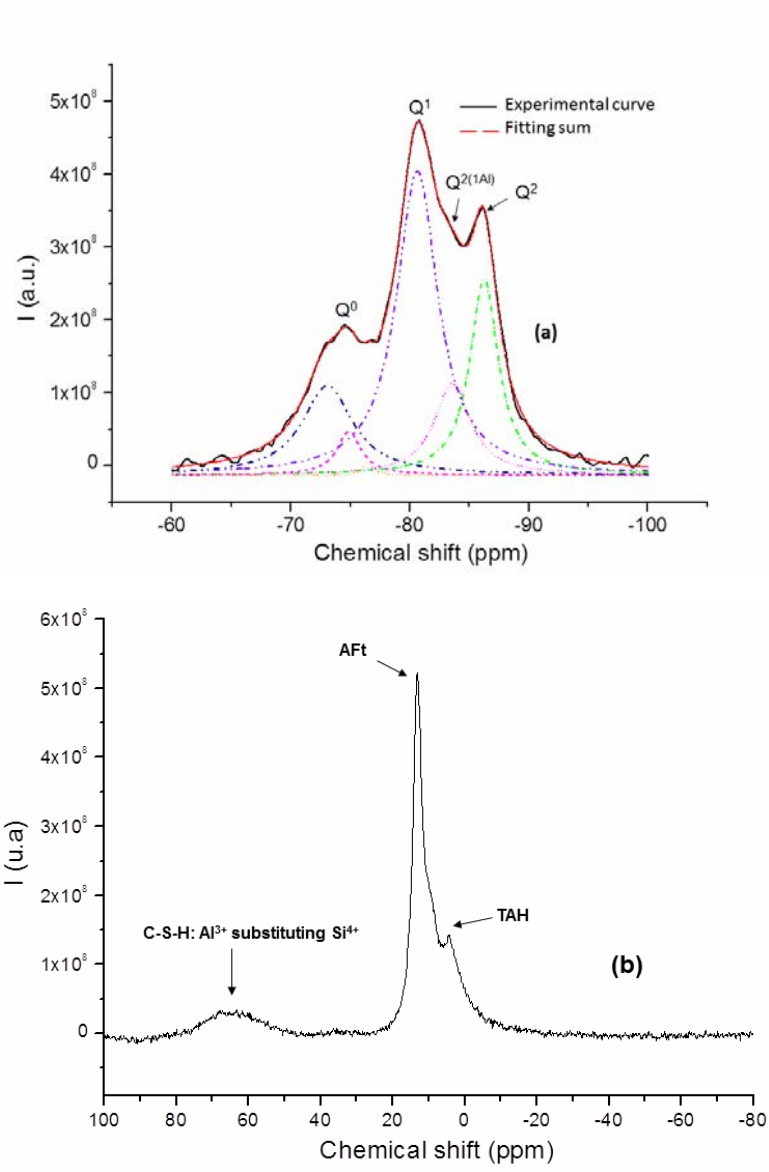

Figure 1. (a) ^{29}Si and (b) ^{27}Al NMR spectra, respectively, for 10N at 28 days.

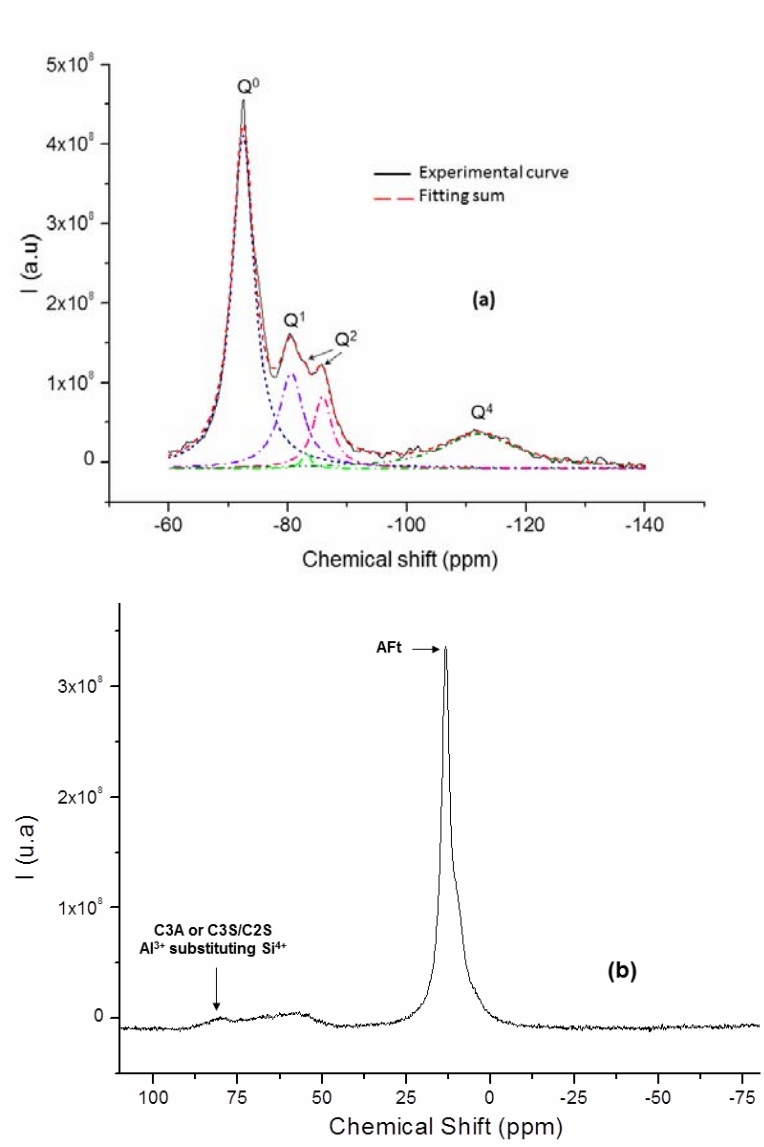

Figure 2. (a) ^{29}Si and (b) ^{27}Al NMR spectra, respectively, for 10NMA at 28 days.

Noticeable differences are observed for samples 10N and 10NMA in the ^{27}Al and ^{29}Si NMR spectra. In the ^{27}Al spectrum for sample 10N, in which the addition of nanosilica was performed over anhydrous cement, three different signals appear. The first one is centered at about 65ppm, typical for aluminum in coordination IV, corresponding to the incorporation of Al^{3+} in the C-S-H gel replacing the Si^{4+}. This fact confirms the interpretation previously given as plausible from that found in the ^{29}Si NMR spectrum: a signal around −82ppm (Figure 1(a)) corresponding to tetrahedral Al^{3+} located in bridging position of the silicate chains [19].

The second signal, centered at 14ppm, corresponds to octahedral coordinated Al^{3+} cations and in this case the signal is ascribed to ettringite [20]. The third signal, appearing around 5ppm, has been assigned before to the replacement of Ca^{2+} located between the C-S-H chains by Al^{3+} or, alternatively, can be related to an Al (VI) species usually called “third-aluminum-hydrate” (TAH). In this case, the small width of the band indicates that the ^{27}Al cations local environment in the TAH component is relatively uniform, as it would be wider if Ca^{2+} would be present [21].

On the other hand, in the ^{27}Al spectrum of the 10NMA sample (Figure 2(b)), in which the addition of nano silica was made on the mixing water, two relevant signals were found. The first one, at ca. 80ppm, corresponds to an isomorphic substitution inverse to the previous case, i.e., Al^{3+} substitution by Si^{4+} in the C3A or in C3S/C2S species [11]. The second signal, centred around 14ppm, corresponds to ettringite, similarly to that indicated above for the 10N sample. It is worth underlining that in the 10NMA sample the signal of Si^{4+} substitution by Al^{3+} in the C-S-H gel does not appear, coherently to the obtained ^{29}Si NMR results, and this fact reveals that the addition method clearly influences the chemical nature of the C-S-H gel. These data show different compositions of the C-S-H gels present in AC and AW samples.

By the deconvolution of 10N and 10NMA ^{29}Si MAS NMR spectra, the values of MCL for both samples have been obtained; these values are 3.40 for 10N and 3.28 for 10NMA. The compositional difference found in the C-S-H gels in both sets of samples, does not provoke any drastic change in this parameter. A possible explanation for this fact is that, for a curing age of 28 days, the Al^{3+} cations are not still incorporated in the bridge positions of the pentamers at high concentration, and this feature is very important for the elongation of C-S-H chains. Some authors have previously shown that the increase in the MCL value also implies an increase in the strength, being these properties very important in the improvement of the service behaviour of these materials [22].

3.2. Infrared spectroscopy (FTIR)

In order to check the possible isomorphic substitution of Si^{4+} by Al^{3+} in the C-S-H gels in the two sets of samples, FTIR measurements in the frequency range $4000-400 cm^{-1}$ were carried out. In Figure 3, the FTIR spectra for the samples 10N and 10NMA at a curing age of 28 days are shown, as representative examples. By detailed analyses of the bands and their displacements in the spectra, it can be determined if the gels formed from the two addition methods employed are different or not. Both spectra show the stretching and bending vibration modes corresponding to O-H groups in H_2O linked to C-S-H gel structure. These vibration modes appear around 3424 and $2920 cm^{-1}$ for stretching, and $1630 cm^{-1}$ for bending. Besides, the stretching vibration mode of the O-H bond of portlandite is also appearing for both samples, around $3642 cm^{-1}$ [23, 24].

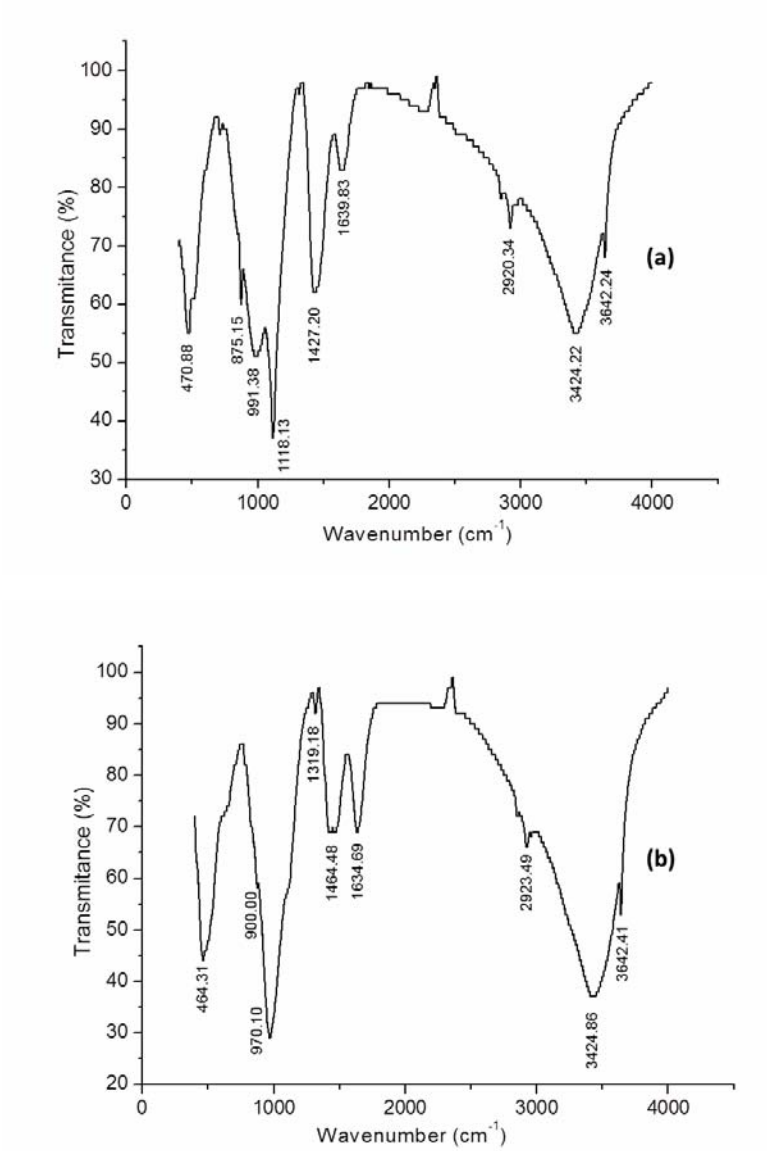

Figure 3. FTIR spectra for (a) 10NMA and (b) 10N.

However, relevant differences can be observed between the spectra gathered in Figure 3, both concerning the frequency range in which the bands appear and the observed intensity of some of them. In this sense, whereas the spectrum of 10NMA sample presents two bands appearing at 875 and 1427cm^{-1}, which correspond to a bending out of plane mode and an asymmetric stretching one of carbonate bonds, respectively, for the 10N sample only the last one is observed, located around 1464cm^{-1} [25]. The apparition of these bands is coherent with their curing age, as stated in literature [26].

On the other hand, it has been established that the vibrations modes corresponding to Si-O bonds, where Si is in tetrahedral coordination, typically appear in the range $400\text{-}1050\text{cm}^{-1}$ [27]. In particular, the energy and position of the band corresponding to asymmetric stretching of Si-O bonds, depend on the introduction of Al ions in Si positions [28]. The bands at 970 and 991cm^{-1}, for 10N and 10NMA, respectively, can be assigned to this signal. The bands corresponding to silicates are shown in Table 3.

Table 3. FTIR spectra Si-O bonds bands for 10N and 10NMA samples

Sample	Vibration modes	Wavenumber (cm^{-1})
10N	In-plane bending Si-O	464
	Asymmetric stretching Si - O Q^2 sites	970
10NMA	In-plane bending Si-O	470
	Stretching Si-O// Stretching S-O	1118
	Asymmetric stretching Si - O Q^2 sites	991

The observed wave number displacement varies inversely with the mean ionic radius of tetrahedrally coordinated cations [29]: the substitution of Al^{3+} by Si^{4+} provokes the shift of the band towards smaller wave number values as the size of $Al^{3+}(0.39\text{Å})$ is greater than

that of $Si^{4+}(0.26Å)$. This suggests that in the 10N sample a fraction of Si^{4+} is replaced by Al^{3+} in the C-S-H chains, causing a displacement in the asymmetric stretching band corresponding to Si-O bond, and this fact supports the results obtained from ^{29}Si and ^{27}Al MAS NMR. In addition, two smaller bands also appear in the 10N FTIR spectrum: a shoulder around $620cm^{-1}$, which can be assigned to Si-O-Al bending vibrations of aluminosilicates [30] and a band around $900cm^{-1}$, which can be attributed to vibrations of Si-O-Al bonds of amorphous aluminosilicates (not present in the 10NMA spectrum, showing that in this case the Si-Al substitution does not take place).

Finally, the band at ca. $1118cm^{-1}$ appearing only in the 10NMA spectrum, could be also ascribed to the above mentioned modifications. In this sense, the absence of this band for the 10N sample could be related to a lack of symmetry in the Si environment as a consequence of the isomorphic substitution process described.

3.3. Mercury intrusion porosimetry (MIP)

In the study of the durability is important to know the possibility of penetration of aggressive agents through the network of pores and capillaries. The distribution of the porosity according to the apparent size of the pores can be obtained from MIP results and, in this way, the porous structure of the material can be characterized [31]. Figures 4 and 5 show the variation of the differential intrusion and the cumulative intrusion versus size pore (in logarithm scale), respectively.

It is well known that additions of micro and nano silica in concretes and mortars improve their mechanical-resistant behaviour, leading to a densification of the microstructure. In this work, we aim to analyse the differences appearing in the microstructure of cement pastes with silica additions focussed on three aspects: concentration, grain size of additions, and mixing method.

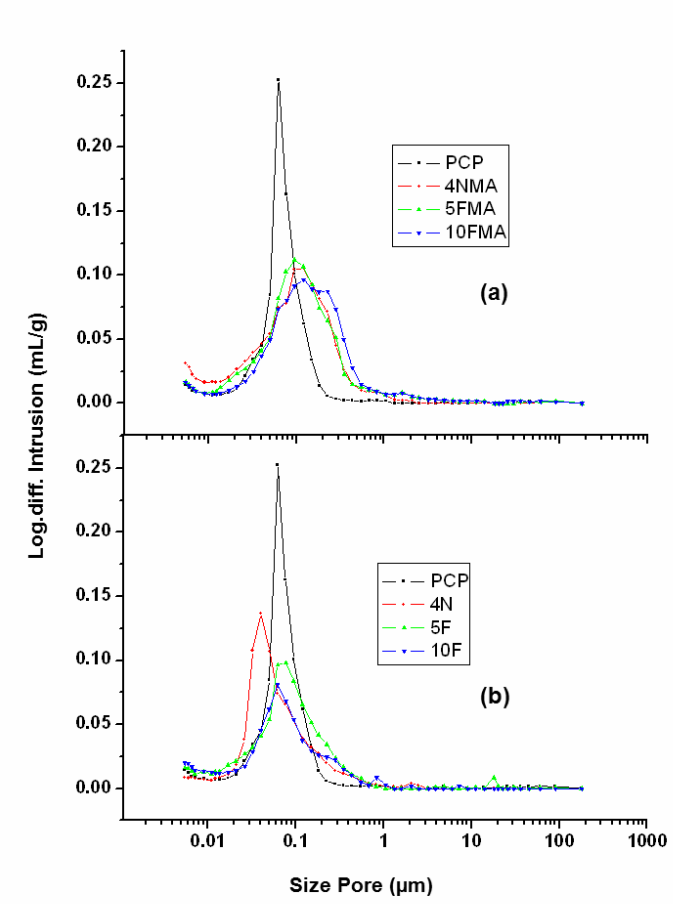

Figure 4. Logarithm differential intrusion vs size pore for (a) AW samples and (b) AC samples.

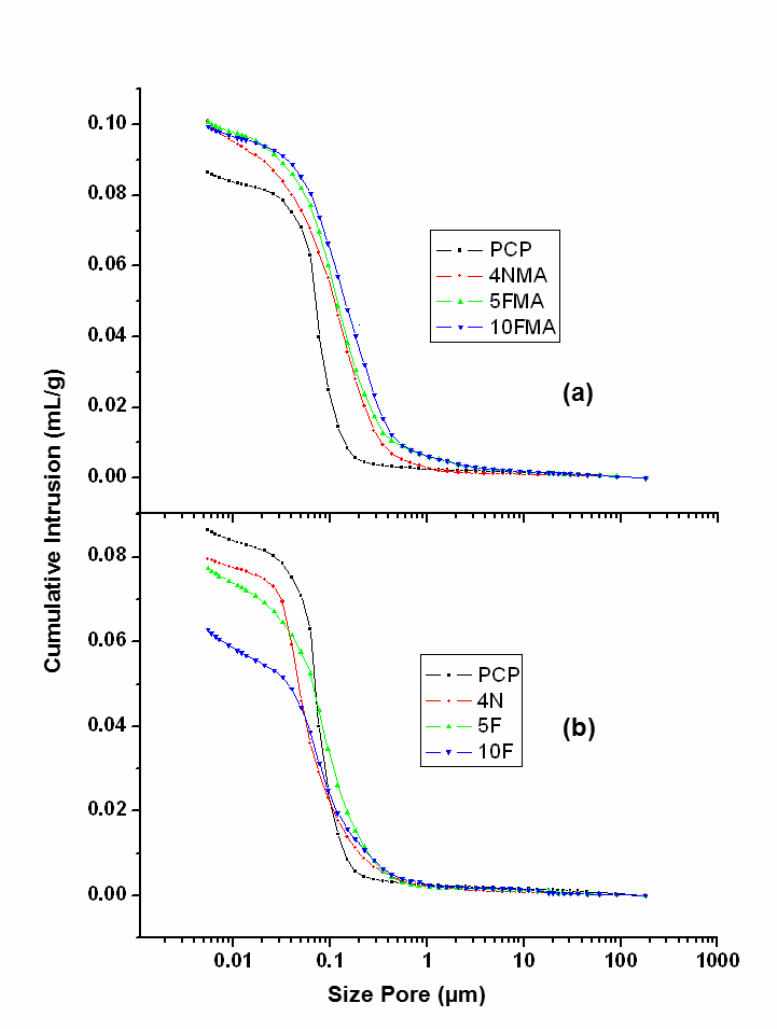

Figure 5. Cumulative intrusion vs size pore (a) AW samples and (b) AC samples.

As it can be observed in Figure 4, the PCP specimen presents a monomodal pore size distribution with one broad peak centered at 0.06μm, ranging from 0.02 to 0.2μm, and this fact evidences a porous structure consisting in capillary pores for this sample [32]. This scenario is drastically changed in samples which incorporate additions and the provoked modifications depend on the addition method.

In the case of the AC samples, all the additions clearly provoke a reduction in pore size (see Figure 4), contrary to that observed for the AW samples, where the value of this parameter remains virtually invariable. However, though the silica fume additions do not improve this aspect of the porous microstructure, it has a significant role in reducing the number of pores. This parameter depends on the percentage of silica fume additions as shown in Figure 4(b).

These results reveal that, when only the densification of the matrix is studied (i.e., in cement pastes), the optimization of microstructure implies a fine tuning of the three aspects investigated. In this sense, it would be interesting to carry out a deeper study, implying a systematic and comparative examination of a greater number of samples.

3.4. Scanning electron microscopy (SEM)

The observed refinement in the porous microstructure of cement pastes with nano silica additions have been previously tested in similar systems [4, 8]. In order to evaluate the microstructure features related to the mechanisms implied in the hydration processes, SEM and EDS experiments were carried out for all of them.

It is generally accepted that the employed nano and microsilica additions from both tested mixing methods lead to a considerable modification of portlandite crystals. Figure 6 comparatively shows selected zones of images for PCP and 4N samples. In this context, the apparition of secondary tobermorite can be followed by analyzing the changes in portlandite crystal morphology and size in the specimens, coherently with the reaction mechanism proposed by Ye Qing et al. [33].

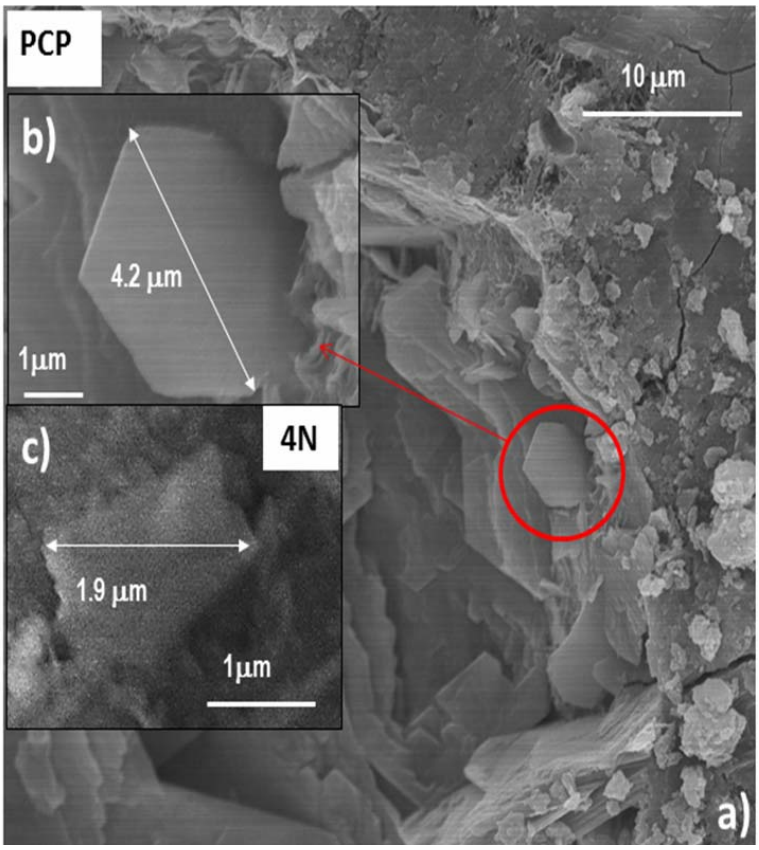

Figure 6. SEM micrographs showing portlandite crystal morphology and size in the (a), (b) PCP sample, and (c) 4N sample.

In addition, Figure 7 shows two representative images for (a), (b) AC and (c) AW samples, respectively. It can be clearly appreciated the presence of aciculate ettringite (AFt) crystals upholstering the pores in the AC samples, whereas their morphology and abundance are very different in the AW specimens. In this sense, the displacement of the diameter pore distribution detected in the AC samples by MIP can be linked to the mechanism of coating the percolated pores.

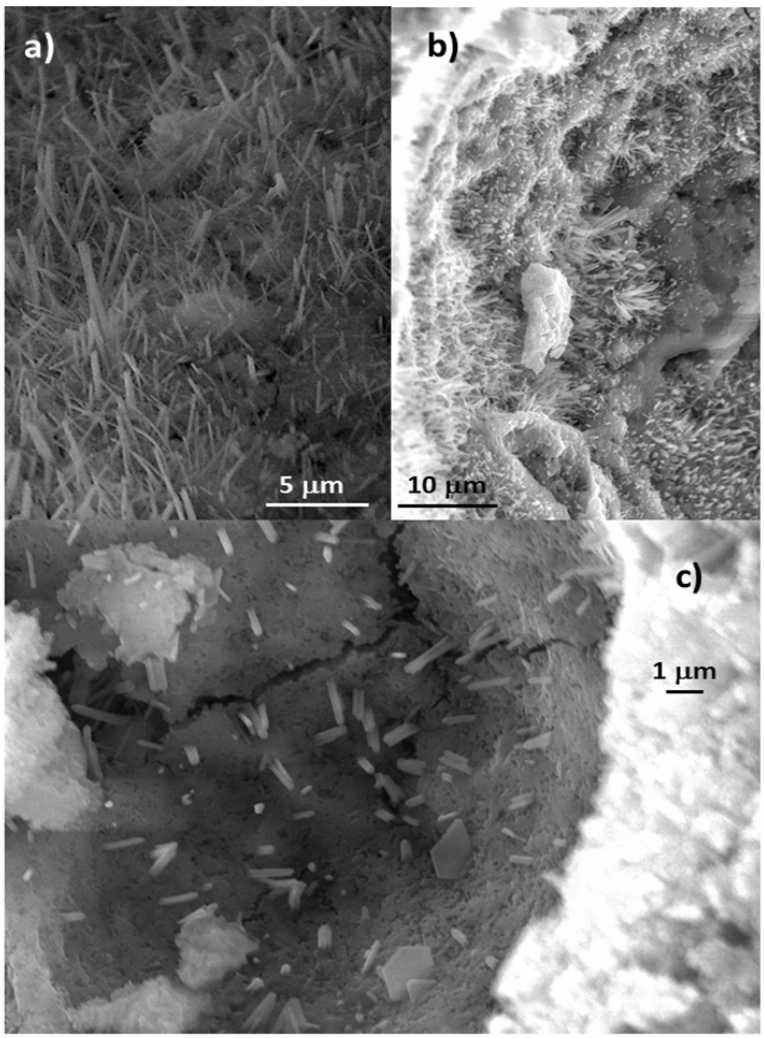

Figure 7. SEM micrographs for (a), (b) AC sample, and (c) AW sample.

On balance this fact can be relevant in aspects such as concrete durability against attack by aggressive agents, i.e., Cl^- or SO_4^{2-}. These results are coherent to those obtained from NMR and MIP experiments.

4. Conclusion

Two sets of nano and microsilica additions cement pastes, prepared by two different mixing methods, have been studied at curing ages of 7 and 28 days. The characterization of the hydration process has been made from ^{29}Si MAS-NMR, ^{27}Al MAS-NMR, FTIR, MIP, EDS, and SEM experiments.

The AC deposition mixing method improves the samples hydration, mean chain length and polymerization parameters, and this has been interpreted in terms of different mechanisms implied in each case.

In the AW samples no isomorphic Al^{3+} substitution in the silicate chains takes place, whereas for the AC samples $Q^2(1Al)$ signals prompted to the existence of aluminosilicate chains. In these chains, the Al^{3+} cations are located in bridging positions of the silicate chains.

Besides, the displacement in the bands corresponding to asymmetric stretching Si-O bond in the FTIR spectra confirm the above mechanisms as it can be interpreted considering a partial replacement of Si^{4+} by Al^{3+} in the C-S-H chains for the AW samples.

Finally, some changes can be observed in the microstructure depending on the mixing method; thus, AC samples present a porous microstructure more refined than AW samples. Moreover, in those pores AFt crystals with aciculated morphology appear upholstering the surface. These facts are confirmed by MIP and SEM, respectively, and indicate promising durability properties.

Acknowledgements

We acknowledge financial support from Spanish Ministerio de Ciencia e Innovación, project ARTIBAL-P07/08 and from Spanish Ministerio de Educación, Cultura y Deporte, project MAT2010-20117. D. Alonso-Domínguez thanks the CEI Moncloa for the concession of a PhD grant**.** Authors are grateful to the CAI centers of UCM (XRD, NMR and electron microscopy).

References

[1] L. P. Singh, K. Agarwal, S. K. Bhattacharyya, U. Sharma and S. Ahalawat, Preparation of silica nanoparticles and its beneficial role in cementitious materials, Nanomater. Nanotechnol. 1 (2011), 44-51.

[2] G. Quercia, G. Hüken and H. J. H. Brouwers, Water demand of amorphous nano silica and its impact on the workability of cement paste, Cem. Concr. Res. 42 (2012), 344-357.

[3] G. Land and D. Stephan, The influence of nano-silica on the hydration of ordinary Portland cement, J. Mater. Sci. 47 (2012), 1011-1017.

[4] I. Campillo, A. Guerrero, J. S. Dolado, A. Porro, J. A. Ibáñez and S. Goñi, Improvement of initial mechanical strength by nanoalumina in belite cements, Mat. Lett. 61 (2007), 1889-1892.

[5] Z. Li, H. Wang, S. He, T. Lu and M. Wang, Investigations on the preparation and mechanical properties of the nanoalumina reinforced cement composite, Mat. Lett. 60 (2006), 356-359.

[6] G. Ming-Zhi, L. Tung-Chai and P. Chi-Sun, TiO_2-based self-compacting glass mortar: Comparison of photocatalytic nitrogen oxide removal and bacteria inactivation, Build. Environ. 53 (2012), 1-6.

[7] H. Li, H. Xiao and J. Ou, A study on mechanical and pressure-sensitive properties of cement mortar with nanophase materials, Cem. Concr. Res. 34 (2004), 435-438.

[8] D. Alonso-Domínguez, A. Moragues, E. Reyes, I. Álvarez-Serrano and C. Pico, Silica-additivated cement pastes obtained from different mixing conditions: Influence on the hydration process, Proceeding VIII Internacional Conference on Fracture Mechanics of Concrete and Concrete Structures (2012).

[9] G. Le Saoût, E. Lécolier, A. Rivereau and H. Zanni, Chemical structure of cement aged at normal and elevated temperatures and pressures, Part II: Low permeability class G oilwell cement, Cem. Concr. Res. 36 (2006), 428-433.

[10] I. G. Richardson, A. R. Brough, R. Brudson, G. W. Groves and C. M. Dobson, Location of aluminum in substituted calcium silicate hydrate (C-S-H) gels as determined by ^{29}Si and ^{27}Al NMR and EELS, J. Am. Ceram. Soc. 79 (1993), 2285-2288.

[11] M. Andersen, H. J. Jakobsen and J. Skibsted, Incorporation of aluminum in the calcium silicate hydrate (C-S-H) of hydrated Portland cements: A high-field ^{27}Al and ^{29}Si MAS NMR investigation, Inorg. Chem. 42 (2003), 2280-2287.

[12] X. Pardal, F. Brunet, T. Charpentier, I. Pochard and A. Nonat, ^{27}Al and ^{29}Si solid-state NMR characterization of calcium-aluminiosilicate-hydrate, Inorg. Chem. 51 (2012), 1827-1836.

[13] J. Schneider, M. A. Cincotto and H. Panepucci, ^{29}Si and ^{27}Al high-resolution NMR characterization of calcium silicate hydrate phases in activated blast-furnace slag pastes, Cem. Concr. Res. 31 (2001), 993-1001.

[14] UNE-EN 196-1: 2005.

[15] ASTM D 4404-84.

[16] M. Andersen, H. J. Jakobsen and J. Skibsted, Characterization of white Portland cement hydration and the C-S-H structure in the presence of sodium aluminate by ^{27}Al and ^{29}Si MAS NMR spectroscopy, Cem. Concr. Res. 34 (2004), 857-868.

[17] I. G. Richardson, J. Skibsted, L. Black and R. J. Kirkpatrick, Characterisation of cement hydrate phases by TEM, NMR and Raman spectroscopy, Adv. Cem. Res. 22 (2010), 233-248.

[18] J. Skibsted and C. Hall, Characterization of cement minerals, cement and their reaction products at atomic and nano scale phases, Cem. Concr. Res. 38 (2008), 205-225.

[19] I. G. Richardson, The nature of C-S-H in hardened cements, Cem. Concr. Res. 29 (1999), 1131-1147.

[20] G. Le Saoût, E. Lécolier, A. Rivereau and H. Zanni, Study of oilwell cements by solid-state NMR, C.R. Chimie 7 (2004), 383-388.

[21] A. Rawal, J. B. Smith, L. G. Athens, L. C. Edwards, L. Roberts, V. Gupta and F. Chmelka, Molecular silicate and aluminate species in anhydrous and hydrated cements, J. Am. Chem. Soc. 132 (2010), 7321-7337.

[22] J. S. Dolado, I. Campillo, E. Erkizia, J. A. Ibañez, A. Porro, A. Guerrero and S. Goñi, Effect of nanosilica additions on belite cement pastes held in sulfate solutions, J. Am. Ceram. Soc. 90 (2007), 3973-3976.

[23] P. A. Bhat and N. C. Debnath, Nanoestructural aspects C-S-H, J. Phys. Chem. Solid 72 (2011), 920-933.

[24] P. Yu, R. J. Kirkpatrick, B. Poe, P. F. McMillan and X. Cong, Structure of calcium silicate hydrate (C-S-H): Near-, mid-, and far-infrared spectroscopy, J. Am. Ceram. Soc. 82 (1999), 742-748.

[25] N. Y. Mostafa, A. A. Shaltout, H. Omar and S. A. Abo-El-Enein, Hydrothermal synthesis and characterization of aluminium and sulphate substituted 1.1nm tobermorites, J. Alloys Compd. 467 (2009), 332-337.

[26] F. Kontoleontos, P. E. Tsakiridis, A. Marinos, V. Kaloidas and M. Katsioti, Influence of colloidal nanosilica on ultrafine cement hydration: Physicochemical and microstructural characterization, Constr. Build. Mater. 35 (2012), 347-360.

[27] V. C. Farmer, The Infrared Spectra of Minerals Edition, Farmer, Mineralogical Society, London, 1974.

[28] Y. Hirata, K. Sakeda, Y. Matsushita, K. Shimada and Y. Ishihara, Characterization and sintering behavior or alkoxide-Derived aluminosilicate powders, J. Am. Ceram. Soc. 57 (1974), 57-61.

[29] P. A. Schroeder, Infrared Spectroscopy in Clay Science: In CMS Workshop Lectures, The Clay Mineral Society Edition, Teaching Clay Science, Aurora, 2002.

[30] M. Nogami, S. Ogawa and K. Nagasaka, Preparation of cordierite glass by the sol-gel process, J. Mat. Sci. 24 (1989), 4339-4342.

[31] L. Cui and J. H. Cahyadi, Permeability and pore structure of OPC paste, Cem. Concr. Res. 31 (2001), 277-282.

[32] S. Mindess, J. Young and D. Darwin, Concrete, 2nd Edition, Pearson Education, Prentice Hall, Inc. Upper Saddle River, 2003.

[33] Y. Qing, Z. Zenan, K. Deyu and C. Rongshen, Influence of nano-SiO_2 addition on properties of hardened cement paste as compared with silica fume, Constr. Build. Mater. 21 (2007), 539-545.

■